
Article:
Da Silva, A.C. orcid.org/0000-0002-6258-9506, Hu, X. orcid.org/0009-0008-3731-2012, Paschoal, V.H. orcid.org/0000-0002-0935-3772 et al. (4 more authors) (2025) Bipolar electrochemistry-driven wireless drug loading and energy harvesting in conductive hybrid hydrogels. Communications Materials, 6 (1). 28. ISSN 2662-4443

https://doi.org/10.1038/s43246-025-00750-1

---

communications materials

A Nature Portfolio journal

Article

https://doi.org/10.1038/s43246-025-00750-1

Bipolar electrochemistry-driven wireless drug loading and energy harvesting in conductive hybrid hydrogels

Aruã Clayton Da Silva [1,2,3,4] ✉, Xiaofeng Hu [1], Vitor Hugo Paschoal [5,6], Nicholas Hagis[1,2,3], Agnieszka Joanna Zajac[1,2,3], Mauro Carlos Costa Ribeiro[5] & Ivan Rusev Minev [1,7,8] ✉

Bipolar electrochemistry enables wireless and spatially controlled redox reactions on (semi) conductive objects immersed in an electrolyte. Here, we investigate advanced bipolar electrochemistry applications using flexible bipolar electrodes coated with hybrid films of conductive polymer poly(3,4-ethylenedioxythiophene) and alginate hydrogels. These coatings allow for the wireless creation of reversible redox and chemical gradients, providing targeted drug loading and energy harvesting opportunities. We use cyclic voltammetry, electrochemical impedance spectroscopy, Raman microscopy, and X-ray photoelectron spectroscopy to characterize distinct redox regions within the bipolar electrode. The wireless and selective loading of a model drug, fluorescein, into the hydrogel, demonstrated control over drug distribution, suggesting an alternative to conventional uniform doping techniques. Furthermore, cutting the gradient-encoded bipolar electrode and closing an external circuit between the halves, enables energy recovery through a concentration cell mechanism. Our findings illustrate the potential of bipolar electrochemistry in creating versatile platforms that bridge materials science, electrochemistry, and bioelectronics for innovative biomedical and energy applications.

Bipolar electrochemistry (BE) is a technique that exploits electric fields to induce polarization in electrolyte-immersed conductive or semi-conductive materials, enabling simultaneous and opposite redox reactions at the extremities of these materials. Essentially, the bipolar electrode (BPE) serves as both an anode and a cathode, with the electric field establishing a potential difference across its length[1]. This wireless approach has been used in several applications to drive electrochemical reactions without direct electrical connections. For example, BE has been employed to perform the electropolymerization of conducting polymer fibers and to create gradient doping in polymer films using a "U"-shaped electrochemical cell[2–7]. This gradient doping effect has enabled advances in bioelectronics, tissue engineering, drug delivery, biosensing, and 3D printing[8–15]. Beyond these fields, BE also finds applications in areas like electroanalysis, motion generation, environmental remediation, and wireless electrostimulation[16–24].

While BE has been extensively explored in various material systems, its use with hydrogels to manipulate their bioactivity, composition, or mechanical properties remains underexplored[25,26]. Prior studies demonstrated that BE could induce localized gel formation in alginate hydrogels, but the potential for gradient-based manipulation of hydrogel properties remains largely untapped[27,28].

In this study, we leverage BE to wirelessly encode reversible gradients of redox state and chemical composition on BPEs comprising layers of poly(3,4-ethylenedioxythiophene) (PEDOT) and Alginate hydrogel. By spatially controlling the redox state, we can create zones of varying chemical reactivity. This enables wireless loading of (fluorescein) molecule

[1]Department of Automatic Control and Systems Engineering, Faculty of Engineering, University of Sheffield, Mappin Street, Sheffield, S1 3JD, UK. [2]Insigneo Institute for in silico Medicine, University of Sheffield, Sheffield, S1 3JD, UK. [3]Sheffield Institute for Translational Neuroscience, University of Sheffield, 385A Glossop Road, Sheffield, S10 2HQ, UK. [4]Department of Chemical Sciences, SSPC the SFI Research Centre for Pharmaceuticals, Bernal Institute, University of Limerick, Castletroy, Limerick, V94 T9PX, Ireland. [5]Laboratório de Espectroscopia Molecular, Departamento de Química Fundamental, Instituto de Química, Universidade de São Paulo, Avenida Professor Lineu Prestes 748, São Paulo, 05508-000, Brazil. [6]Soft-Matter Optics Group, Faculty of Chemistry, Wrocław University of Science and Technology, Wybrzeże Wyspiańskiego 27, Wrocław, 50-370, Poland. [7]Else Kröner Fresenius Center for Digital Health, Faculty of Medicine Carl Gustav Carus, TUD Dresden University of Technology, Fetscherstr. 74, 01307 Dresden, Germany. [8]Leibniz Institute of Polymer Research Dresden, Hohe Strasse 6, Dresden, 01069, Germany. ✉e-mail: Arua.DaSilva@ul.ie; minev@ipfdd.de

concentration gradients in the hydrogel and PEDOT layers. Our approach creates opportunities in two main areas: drug delivery and energy harvesting. For example, gradient-encoded BPEs were removed from solution and cut in half to prevent re-equilibration by diffusion. We demonstrated that by closing an electronic circuit between the two (electrolyte immersed) halves, some of the energy stored in the gradient can be recovered. By capitalizing on the unique capabilities of BE, our work presents a promising strategy to enhance processes of wireless energy harvesting and wireless drug loading.

Results and discussion

Conducting polymer films and bipolar electrochemistry

We begin by preparing films of PEDOT deposited on ITO/PET substrates via electropolymerization +2.0 V (vs Ag/AgCl/KCl 3 M) in an aqueous solution of 3,4-ethylenedioxythiophene (EDOT) (50 mmol) and sodium dodecyl sulfate (SDS) (70 mM) in a standard 3-electrode electrochemical cell (Supplementary Fig. 1). After the conducting polymer PEDOT is electrodeposited, the ITO/PET/PEDOT stack serves as the BPE in subsequent BE experiments (Fig. 1).

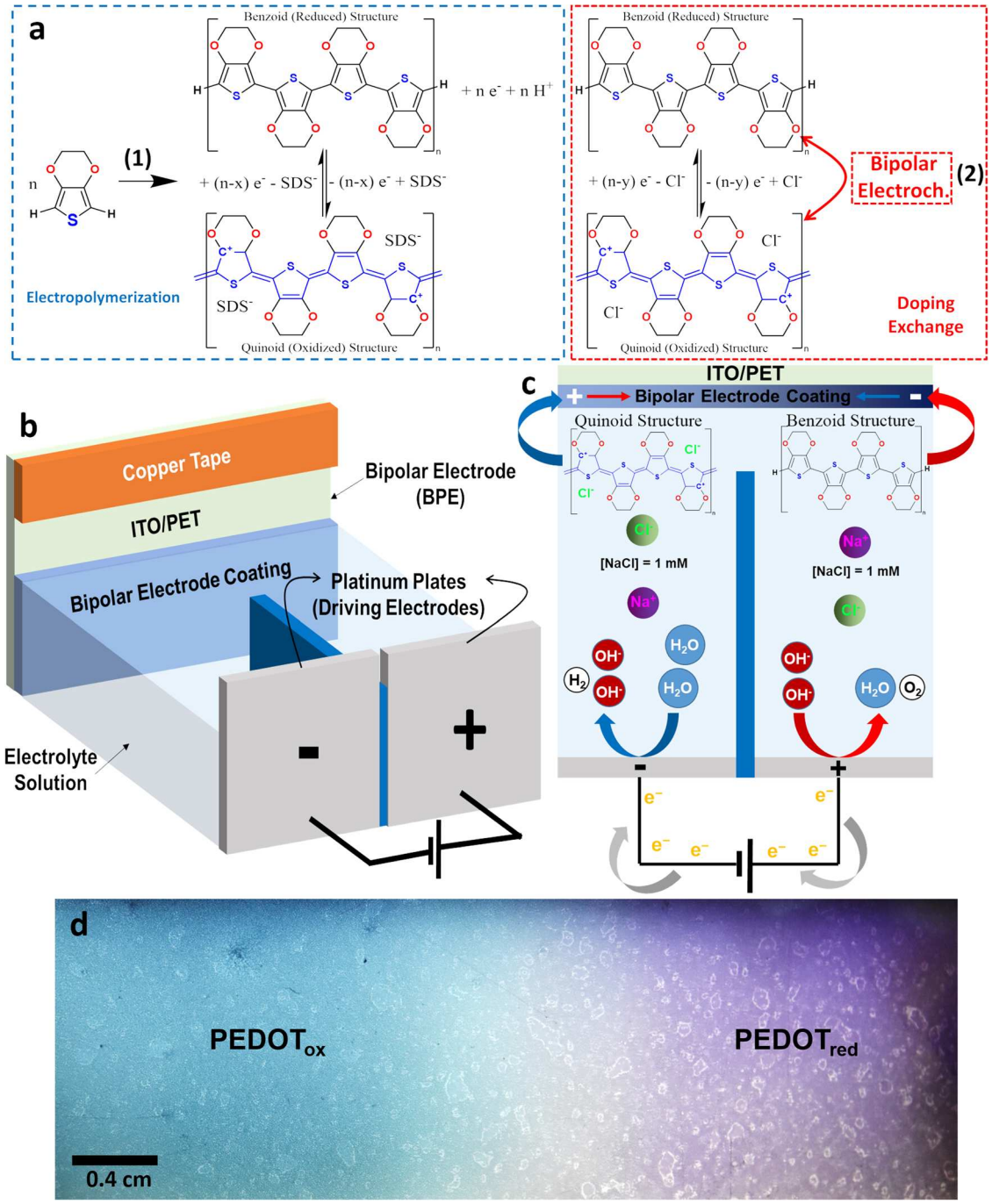

Fig. 1 | Conducting Polymer Films and Bipolar Electrochemistry. a Chemical reactions involving the electropolymerization of EDOT (blue dashed square), resulting in a mixture of neutral PEDOT (benzoid structure) and oxidized PEDOT (quinoid structure, depicted in blue). The redox equilibrium can be controlled via bipolar (wireless) electrochemistry (red dashed square). **b** Schematic representation of the bipolar electrochemical cell, where the PEDOT film electrodeposited on a flexible ITO/PET substrate serves as the BPE. **c** Top-view schematic representation of the bipolar electrochemical cell: water hydrolysis reactions at the driving electrodes are depicted on each side, while the redox reaction of PEDOT occurs at the BPE. **d** Image of the PEDOT film after the bipolar activation: oxidized PEDOT on the left and reduced PEDOT on the right.

Figure 1a illustrates the initial electropolymerization of the PEDOT film and its subsequent switching during BE experiments. Initially, EDOT monomers undergo electropolymerization to form PEDOT with a mixture between benzoid and quinoid structures (step 1, blue). Subsequently, the redox electrochemical reaction of PEDOT, transitioning between the benzoid and quinoid states, can be regulated by the bipolar (wireless) electrochemical process (step 2, red). The lack of direct wiring in BE simplifies the experimental setup, especially for BPEs with complex geometries or stacks of multiple (semi)conductive materials. Simplifying the connectorization challenge thus may open new possibilities for flexible electronics or implantable systems. The BE process could further enable: (1) the loading of additional dopant into the oxidized side, and (2) the enhancement of conductivity in the oxidized side of the conducting polymer. Unlike conventional electrochemistry, which often operates under single polarity, BE activation enables simultaneous oxidation and reduction reactions to take place on a continuous (semi)conductive surface.

Figure 1b depicts the schematic representation of the bipolar electrochemical cell. As driving electrodes (DEs) we employ two platinum plates. As illustrated in Fig. 1c, the bipolar cell has a "U" shape configuration and is filled with a supporting electrolyte solution. Chronopotentiometry (CP) is employed over the DEs, wherein a controlled current density (±1.0 mA/cm^2) is applied until a pre-set charge is reached. At the negative electrode, two water molecules accept two electrons, resulting in the generation of hydrogen gas and two hydroxide ions. Conversely, at the positive electrode, hydroxide ions undergo a reaction, yielding half oxygen gas, water molecules, and two electrons. The supporting electrolyte is 1 mM sodium chloride. Chloride ions contribute to the PEDOT redox reaction as co-dopants. The BE activation naturally creates a gradient of oxidation and reduction along the BPE. Figure 1d presents the effect of BE activation on the PEDOT layer (0.6 C passed through the driving electrodes). On the left, the oxidized PEDOT is light blue, while the right side reduced PEDOT shows a dark blue/purple hue. In BE activation experiments, we identified an upper limit of 1.2 C. Beyond this, we observed reduction in the ITO layer of the BPE, resulting in loss of its conductivity (Supplementary Fig. 2)

Doped PEDOT films as BPE

We investigated PEDOT BPEs prepared using either TPP (tripolyphosphate, 150 mM) or SDS (sodium dodecyl sulfate, 70 mM) during the initial electropolymerization step. Both SDS and TPP doped BPEs displayed color gradients in the bipolar electrochemical cell. Figure 2a displays optical microscope images of the PEDOT:SDS BPE subjected to four charge cycles in the bipolar electrochemical cell. On the left, the pristine PEDOT:SDS exhibits a light blue color. In the first cycle (0.3 C passed through the driving electrodes), the top portion displays a light blue hue indicative of PEDOT:SDS$_{ox}$, while the bottom exhibits a dark blue/purple color representing PEDOT:SDS$_{red}$. Conversely, in the second cycle (0.3 C passed in the opposite direction), the top appears dark blue for PEDOT:SDS$_{red}$, while the bottom appears light blue for PEDOT:SDS$_{ox}$. Similar color variations are observed in the subsequent 3rd and 4th cycles, albeit with varying intensities. At the conclusion of the 9th cycle, the ITO layer becomes damaged. Brown discoloration at the edges (similar to Supplementary Fig. 2) is indicative of conductivity loss due to irreversible reduction of the ITO layer[29]. CP data for the bipolar activation setup (obtained when cycling a PEDOT:SDS BPE) is provided in Supplementary Fig. 3 and Supplementary Movie 1.

The BPE was cut in two halves (perpendicular to the redox gradient) and the halves were studied using electrochemical methods. Figure 2b presents CVs of the BPE halves for both TPP and SDS doped systems. SDS doping demonstrated enhanced electroactivity as compared to the TPP ion and was selected for further experiments[30]. As expected, the oxidized halves displayed larger charge storage capacity as observable during CV. Interestingly both the reduced and oxidized halves exhibited improved conductivity after BE activation (see Supplementary Fig. 4). This may be attributed to structural changes induced by the presence of Cl^- ions as additional co-dopant during the BE experiment. Figure 2c depicts EIS Nyquist plots for BPE halves for both TPP and SDS systems. Consistent with the observations in the CV, the EIS data reveals lower impedance for the oxidized halves of the BPEs. Figure 2d illustrates the modified Randles equivalent circuit utilized for modeling the electrical properties derived from EIS. Additionally, Fig. 2e presents a table containing all the EIS parameters extracted from the equivalent circuits. For BPE halves containing either PEDOT:SDS or PEDOT:TPP, the oxidized surface demonstrates lower resistance in comparison to the reduced surface. The PEDOT:SDS system exhibits lower resistance than PEDOT:TPP, consistent with the observations from CV (see Fig. 2b). Taken together these observations demonstrate the effectiveness of BE to wirelessly encode differences in the electrochemical properties of redox active conductive surfaces.

Spectroscopic analysis of BPEs

In addition to the electrochemical characterization, we studied BPEs (PEDOT:SDS layer) through Raman and XPS spectroscopy, as depicted in Fig. 3. Figure 3a displays optical images of the regions of PEDOT:SDS$_{ox}$ and PEDOT:SDS$_{red}$ where the spectra were obtained. Figure 3b illustrates the chemical structure of the benzoid and quinoid forms, highlighting the structural variances (black arrows) at the C_α=C_β position. Figure 3c contains representative Raman spectra for PEDOT:SDS$_{ox}$ (light blue) and PEDOT:SDS$_{red}$ (dark blue). These spectra predominantly feature bands associated with deformations of the ethylenedioxythiophene ring, particularly the deformations of the C–C and C=C bonds in non-oxidized, polaronic, and bipolaronic PEDOT chains, which exhibit significant Raman cross-sections[31]. In this context, the most prominent band at approximately 1422 cm^{-1} (highlighted in gray region) indicates the C_α=C_β (symm. str.)[31–34]. Additionally, the shift of the main peak (observable in the inset), suggests that PEDOT:SDS$_{ox}$ contains more quinoid structures compared to PEDOT:SDS$_{red}$. The presence of a pronounced shoulder for PEDOT:SDS$_{red}$ at approximately 1553 cm^{-1} (highlighted in red) is indicative of the benzoid form. The scattered intensity at the 1553 cm^{-1} shoulder is decreased on the oxidized (quinoid) side of the BPE. Here we normalized the spectra intensity by the height of the main peak in 1422 cm^{-1}, therefore the differences in the shoulders can be better compared. Figure 3d displays the XPS spectra for C 1s (top), O 1s (middle), and S 2p (bottom) for PEDOT:SDS$_{ox}$ (left, light blue frame) and PEDOT:SDS$_{red}$ (right, dark blue frame). In the C 1s spectra, higher intensities are observed for the C–C, C=C, and C–S bonds in PEDOT:SDS$_{red}$. Similarly, the O 1s spectra exhibit higher intensities for more oxidized groups in PEDOT:SDS$_{red}$. Lastly, the S 2p spectra show significantly higher intensity in the SDS region for PEDOT:SDS$_{red}$[35,36]. It suggests that PEDOT:SDS$_{red}$ contains a higher amount of SDS dopant compared to PEDOT:SDS$_{ox}$. Although this result may appear counter-intuitive, during the bipolar activation, the SDS dopant could be exchanged for chloride ions from the electrolyte. Consequently, although some SDS remains incorporated into the pristine PEDOT structure, chloride ions are incorporated into PEDOT:SDS$_{ox}$ after the bipolar activation (see Supplementary Fig. 5). This is consistent with the enhancement of electrochemical properties, observed in Fig. 2. Additionally, by employing XPS analysis to assess surface composition (atomic%), we estimated that the PEDOT:SDS$_{ox}$ structure contains one SDS molecule for every five EDOT monomers in the PEDOT conducting polymer, as proposed in Supplementary Fig. 6.

Hybrid hydrogel coating as BPEs

Next, we investigated complex BPE structures incorporating an ionically conductive hydrogel coating (Fig. 4). These hybrid BPEs consist of PET/ITO/PEDOT/Alginate layers. Here PEDOT and Alginate are formed in a single-step process in a standard 3-electrode electrochemical cell[37]. Initially, EDOT monomers undergo electropolymerization to form PEDOT with benzoid and quinoid structures. Protons (H^+) generated during this process catalyze calcium carbonate decomposition, releasing calcium ions at the electrochemical interface. These ions, along with dissolved alginate, facilitate natural hydrogel assembly at the interface (Fig. 4a, steps 2 and 3). Well-adherent hydrogel coatings with millimeter thickness can be produced in this way as illustrated in the cross section in Fig. 4bi. After fabrication, the hybrid BPEs were tested in a bipolar electrochemical cell as before (±0.6 C

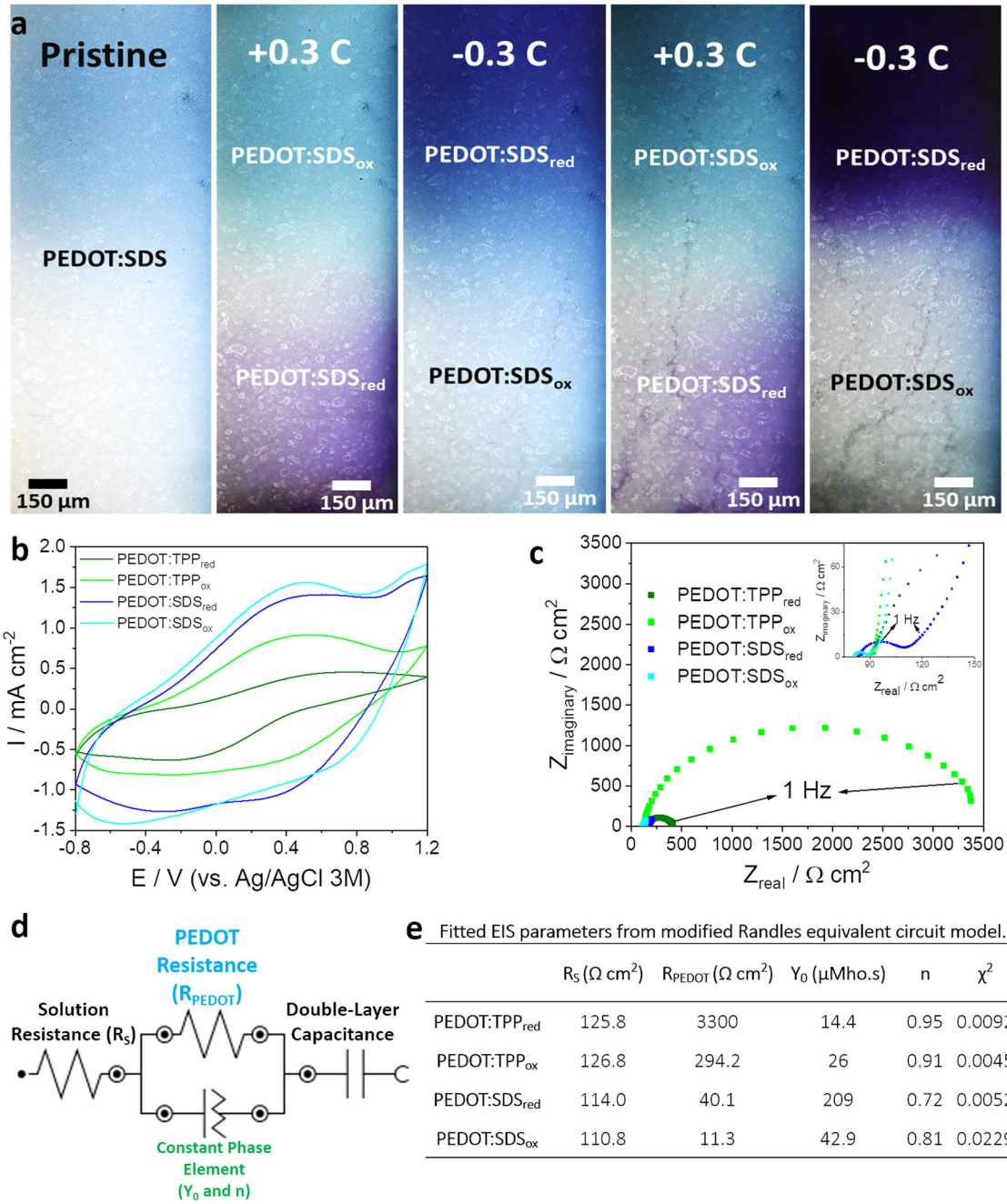

e Fitted EIS parameters from modified Randles equivalent circuit model.

	R_S (Ω cm^2)	R_{PEDOT} (Ω cm^2)	Y_0 (µMho.s)	n	χ^2
PEDOT:TPP$_{red}$	125.8	3300	14.4	0.95	0.0092
PEDOT:TPP$_{ox}$	126.8	294.2	26	0.91	0.0045
PEDOT:SDS$_{red}$	114.0	40.1	209	0.72	0.0052
PEDOT:SDS$_{ox}$	110.8	11.3	42.9	0.81	0.0229

Fig. 2 | Doped PEDOT Films as BPE. a Optical microscope images of pristine PEDOT:SDS films followed by BE activation implemented by applying ±0.3 C via the driving electrodes. Any color non-uniformity in the pristine film is quickly overwritten by BE activation. **b** Cyclic voltammetries (CV) of reduced and oxidized BPE halves. Comparative 10th cycle of CV for PEDOT doped with either SDS or tripolyphosphate (TPP), recorded in phosphate-buffered saline (PBS) at 50 mV s^{-1}. **c** Electrochemical impedance spectroscopy (EIS) of reduced and oxidized BPE halves. Nyquist plot of EIS for PEDOT doped with either SDS or TPP, recorded in PBS solution. Inset: Higher magnification of the Nyquist plot. **d** Modified Randles equivalent circuit used to model the electrical properties of the interface. R_S indicates solution resistance, R_{PEDOT} is the electronic resistance of PEDOT, and CPE represents the constant phase element containing Y_0 as the CPE parameter ($Y{\cdot}\omega^n$), where Y is admittance, ω is frequency, and n is the deviation from ideal capacitive behavior; and double-layer capacitance[46]. **e** Table showing values of putative electronic components in the proposed equivalent circuit. These values were obtained by fitting the circuit to EIS spectra.

delivered via the DEs), also see Supplementary Fig. 7. Figure 4bii shows a hybrid BPE after the bipolar activation. The hybrid BPEs showed no color change due to their thicker, opaque PEDOT layer. Following cutting the BPE as before, significant differences in electrochemical properties between oxidized (PEDOT/Alginate$_{ox}$) and reduced (PEDOT/Alginate$_{red}$) halves were observed (Fig. 4c–e). We evaluated the charge storage capability following three cycles of bipolar activation, demonstrating consistent performance without significant coating changes (Fig. 4f). Gravimetric analysis revealed no statistically significant differences between the oxidized and reduced hydrogels in the wet state, although PEDOT/Alginate$_{ox}$ exhibited slightly lower mass in the dried state (Fig. 4g). Water content analysis indicated slightly higher content in PEDOT/Alginate$_{ox}$, likely due to higher swelling caused by the presence of more positive charges (Fig. 4h).

Wireless loading of small molecules

Hydrogel biomaterials are widely recognized for their potential as biomaterials for drug delivery, however encoding spatial concentration

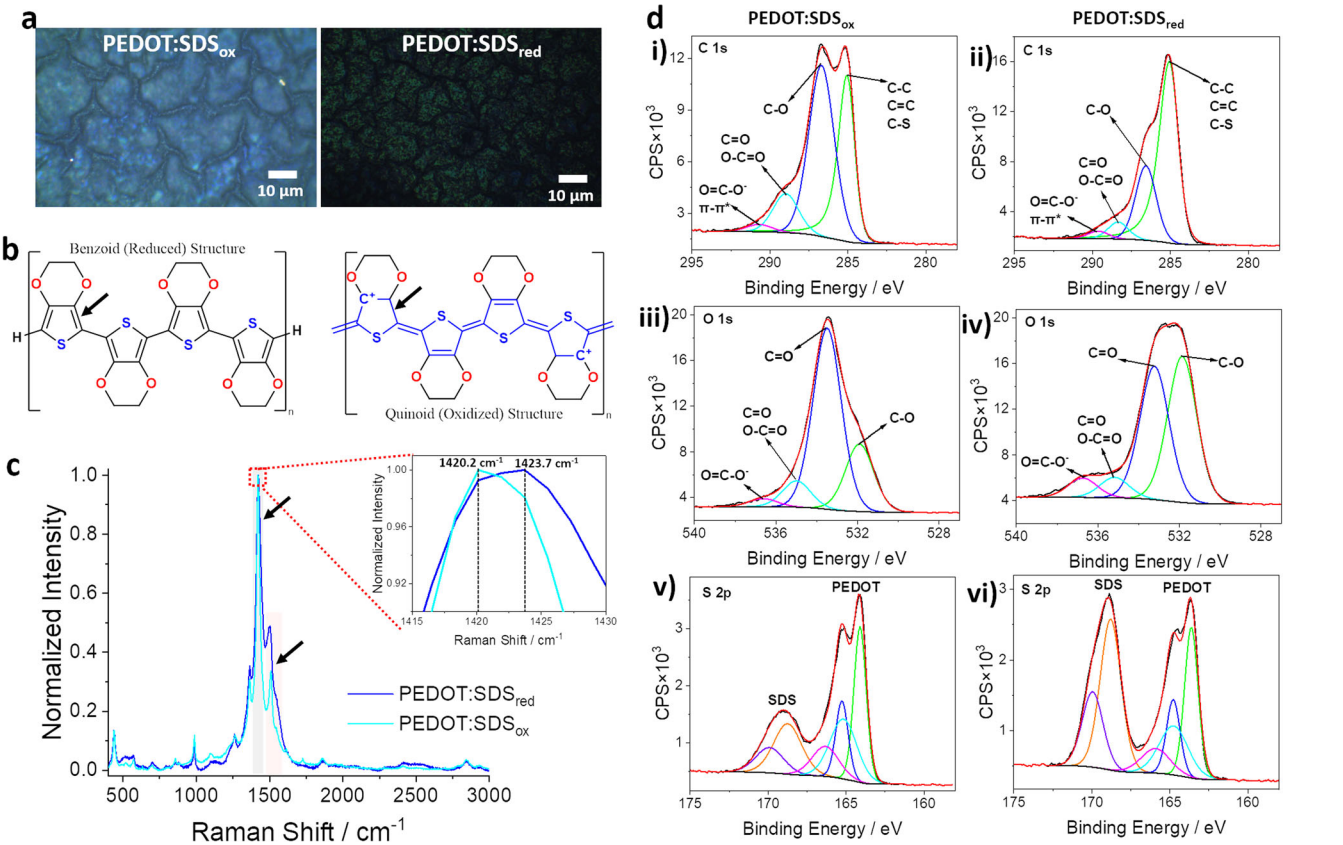

Fig. 3 | Spectroscopic analysis of BPEs. a Optical microscope images of the oxidized (left) and reduced (right) PEDOT:SDS regions where Raman spectra were acquired. **b** Structural differences between the benzoid and quinoid forms of PEDOT, with arrows indicating the differences in the bonds of Cα and Cβ atoms in the thiophene ring. **c** Raman spectra of the oxidized (light blue) and reduced (dark blue) PEDOT:SDS regions. The gray shading highlights the main peak at 1422 cm^{-1} (Cα=Cβ symmetric), and the red shading shows a shoulder at 1553 cm^{-1} (Cα=Cβ asymmetric). Inset: details of the main peak region. **d** X-ray photoelectron spectroscopy (XPS) spectra of oxidized (left column) and reduced (right column) PEDOT:SDS regions, respectively. Spectra include the C 1s (**i** and **ii**), O 1s (**iii** and **iv**), and S 2p (**v** and **vi**) regions for each sample.

gradients of the loaded cargo is challenging[37]. Here we explored if the BPE can be wirelessly loaded with a gradient of a model drug molecule. Fluorescein was chosen for its small size and electronegativity which enables it to enter the alginate layer and act as dopant of the PEDOT layer of the BPE coating. Thus, instead of sodium chloride, we used fluorescein sodium salt at a concentration of 1 mg mL^{-1} as electrolyte (loading solution) in the BE cell, (Supplementary Movie 2). Figure 5ai illustrates the initial state of the BPE following wireless loading of fluorescein. We expect that the two halves (PEDOT/Alginate$_{ox}$ and PEDOT/Alginate$_{red}$) will release different amounts of fluorescein when separately placed in PBS. Further we differentiate between two mechanisms of release. Figure 5aii depicts the passive (diffusion-controlled) release of fluorescein from the Alginate hydrogel, likely involving molecules loosely bound to the hydrogel matrix or repelled by negatively charged alginate macromolecules. Figure 5aiii illustrates the electroactive (electric potential-controlled) release, where fluorescein incorporated into the PEDOT layer is released upon applying a negative electric potential. In agreement with expectations, the oxidized half of the BPE released more fluorescein than the reduced half (Fig. 5b). The initial fluorescein concentration in the Alginate layer was estimated to be 3.1 mg/mL for the oxidized half and 2.2 mg/mL for the reduced half. This indicates that BE sets up a small concentration gradient in the Alginate layer of the BPE. Figure 5c shows the evolution of the Nyquist plot from EIS of the oxidized half of the BPE as a function of immersion time in PBS. As fluorescein leaves the alginate layer, both imaginary and real impedances increase. Figure 5d presents the fluorescein release profile alongside impedance modulus at 1 Hz. Increased impedance may thus serve as an indirect indicator of fluorescein release. As discussed previously, BE activation can replace some dopants incorporated during PEDOT polymerization with a co-dopant from the BE electrolyte. This leads to the expectation that some of the fluorescein will be incorporated as co-dopant in the PEDOT layer of the BPE. Thus, following passive release from the Alginate layer, we applied negative electric potentials to release this residual amount of fluorescein (Supplementary Fig. 8). As illustrated in Fig. 5e, upon electrical stimulation, the oxidized half of the BPE released more fluorescein than the reduced half. The amounts released via electrically driven processes are significantly smaller than those released during passive diffusion which can be explained by the relative sizes of the Alginate and PEDOT layers. Our results however show that fluorescein concentration gradients are preserved in both the PEDOT and Alginate layers of the BPE. Figure 5f illustrates the electroactive release profile from the oxidized half of the BPE (PEDOT/Alginate$_{ox}$). A constant electric potential of −0.8 V (vs Ag/AgCl/KCl 3 M) results in faster release, as compared to a protocol of pulsed electrode polarization (4 min duty cycle, 8 s at −0.8 V followed by 232 s at OCP).

In summary, we demonstrated two distinct modes of model drug release from BPEs. During passive diffusion, an initial burst release occurs, followed by a slower, gradual release as equilibrium is reached, limiting the ability to precisely control the release kinetics. Electrically stimulated release on the other hand may enable a more consistent and adjustable release profile. The layered architecture of our BPEs may be advantageous in potential future applications. For example, the PEDOT layer may serve as controllable source of biomolecular gradients, while the overlaying hydrogel layer may host a 3D culture of biological cells or organoids.

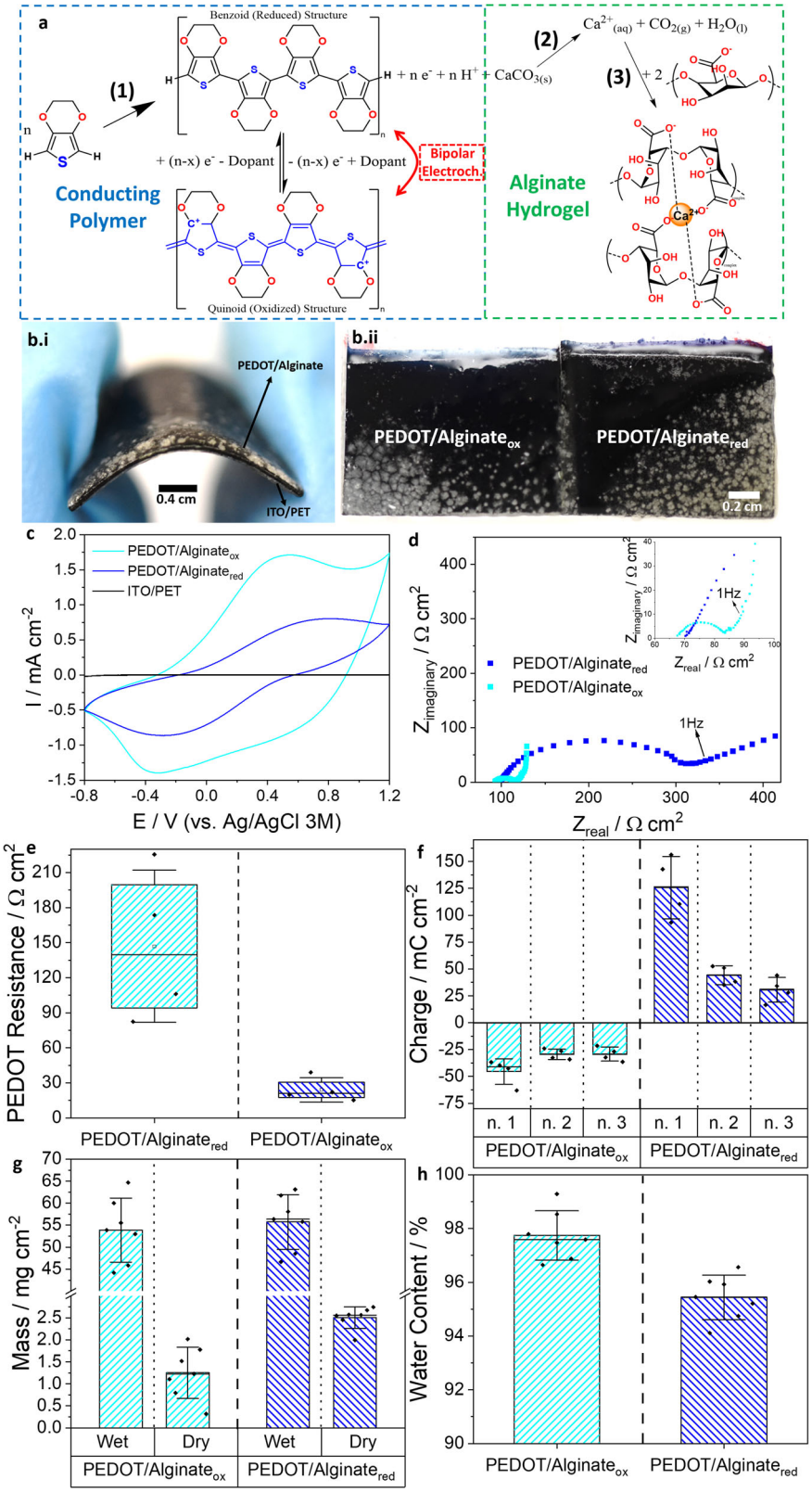

Fig. 4 | Hybrid Hydrogel Coating as BPEs. **a** Chemical reactions involved in single-step electrodeposition of the conductive hybrid hydrogel: (1) Electropolymerization of EDOT (blue dashed square) to the mixture between neutral state of PEDOT (benzoid structure) and oxidized PEDOT (quinoid structure, represented in blue). PEDOT electro polymerization takes place in parallel with (2) decomposition of calcium carbonate, and (3) complexation with alginate macromolecules, resulting in formation of the alginate hydrogel (green dashed square). The redox equilibrium of PEDOT can be subsequently controlled by bipolar (wireless) electrochemistry. **b** Pictures of: (i) the entire BPE subjected to bending, and (ii) the oxidized (left) and reduced (right) sides following BE activation. **c** The 10th cycle of CV for the bare ITO/PET (black), PEDOT/Alginate$_{ox}$ (light blue) and PEDOT/Alginate$_{red}$ (dark blue), recorded in PBS at 50 mV s^{-1}. **d** Nyquist plot of EIS for the PEDOT/Alginate$_{ox}$ (light blue) and PEDOT/Alginate$_{red}$ (dark blue), recorded in PBS. **e** PEDOT resistance obtained from EIS for oxidized (right) and reduced (left) halves. **f** Charge storage capacity of reduced and oxidized BPE halves was obtained by applying +1.2 V or −0.8 V (vs Ag/AgCl/KCl 3 M) respectively for 30 min while measuring the resulting currents. Later, the BPEs were electronically reconnected using a new copper tape and placed back in the bipolar electrochemical cell as BPE electrode for a new cycle (n. 1, 2 and 3). **g** Wet mass (left) and dry (right) mass of hydrogels in the oxidized (light blue) and reduced (dark blue) halves of the BPE. **h** Water content in the oxidized (light blue) and reduced (dark blue) halves of the BPE. Error bars in (**e**–**h**) are standard deviations (see "Methods").

Wirelessly charged concentration cell battery

Concentration cell batteries are well-known electrochemical systems that generate electrical energy from ionic gradients. Various studies have demonstrated their versatility and efficiency in diverse applications, including pH-dependent systems and dual-electrode designs using redox-active materials[38–40]. Since the BE process can asymmetrically distribute small dopant ions (Cl^-) along the PEDOT and Alginate layers, a potential application of wirelessly charged BPEs is in energy harvesting (Fig. 6). When the BPE is cut in the middle and the two halves are immersed in the same electrolyte, the re-establishment of ionic equilibrium is accompanied by electron flow in an external electronic circuit (Fig. 6a). In other words, the higher concentration of ions in the oxidized

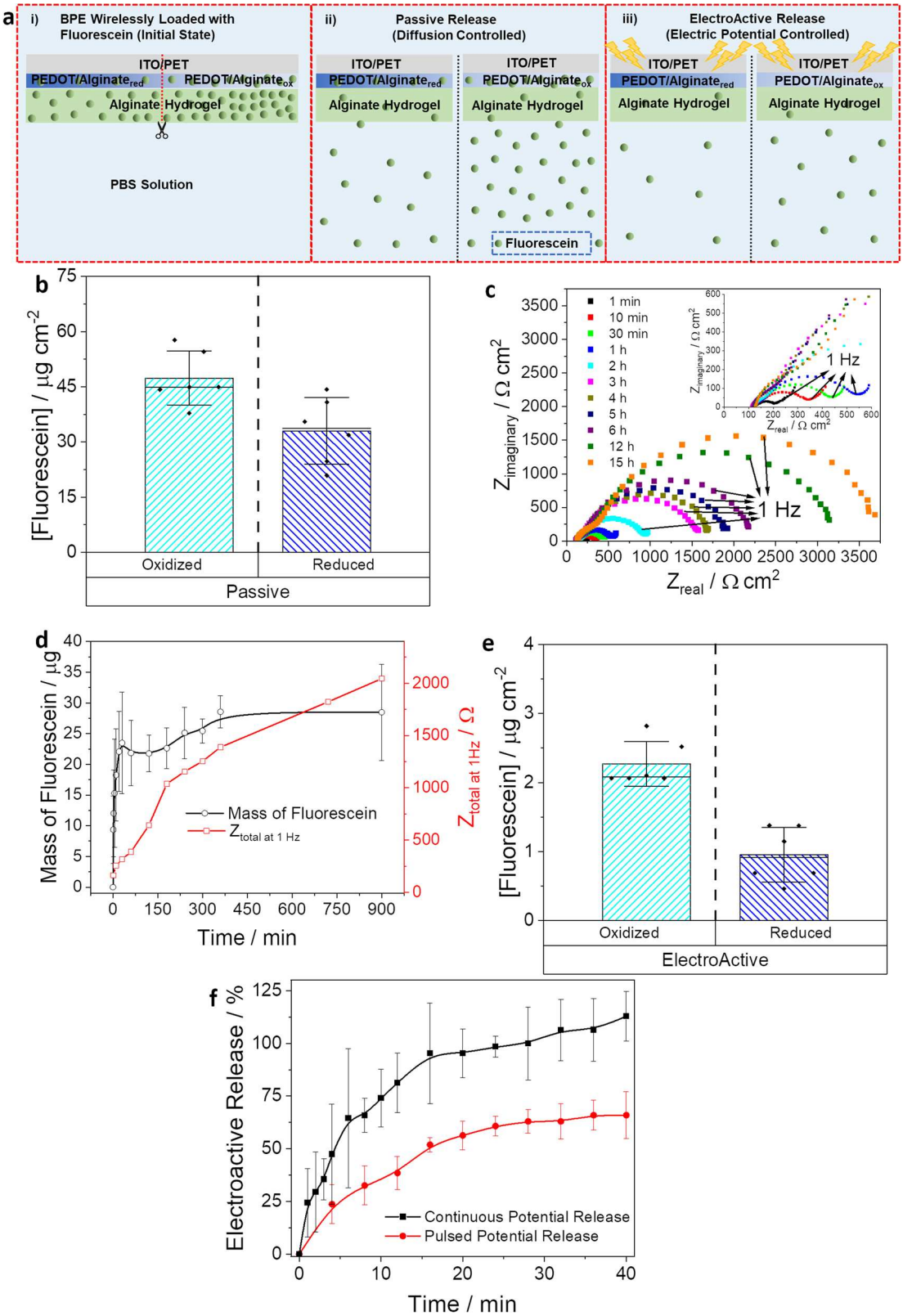

Fig. 5 | Wireless Loading of Small Molecules. a Schematic representation of the BPE (PET/ITO/PEDOT/Alginate hydrogel) wirelessly loaded with fluorescein molecules (red dashed square), where **(i)** represents the initial state of the intact BPE fully loaded with fluorescein molecules, **(ii)** represents passive (diffusion-controlled), and **(iii)** electrically controlled release from Alginate and PEDOT layers of the BPE halves. **b** Concentration of fluorescein passively released from the oxidized (light blue) and reduced (dark blue) halves of the BPE. **c** Nyquist EIS plots of a BPE (oxidized half) during passive fluorescein release. **d** Passive release profile (black, $n = 4$) and total impedance (red, $n = 1$) vs time for the oxidized half of a BPE. **e** Quantification of electrically driven release from oxidized (light blue) and reduced (dark blue) halves of a BPE. **f** Profile of electrically driven release from the oxidized half of a BPE. Application of continuous −0.8 V (vs Ag/AgCl/KCl 3 M) or pulsed (8 s at −0.8 V) potential results in control of the release kinetics, $n = 3$. Error bars in **b**, **d**–**f** are standard deviations (see "Methods").

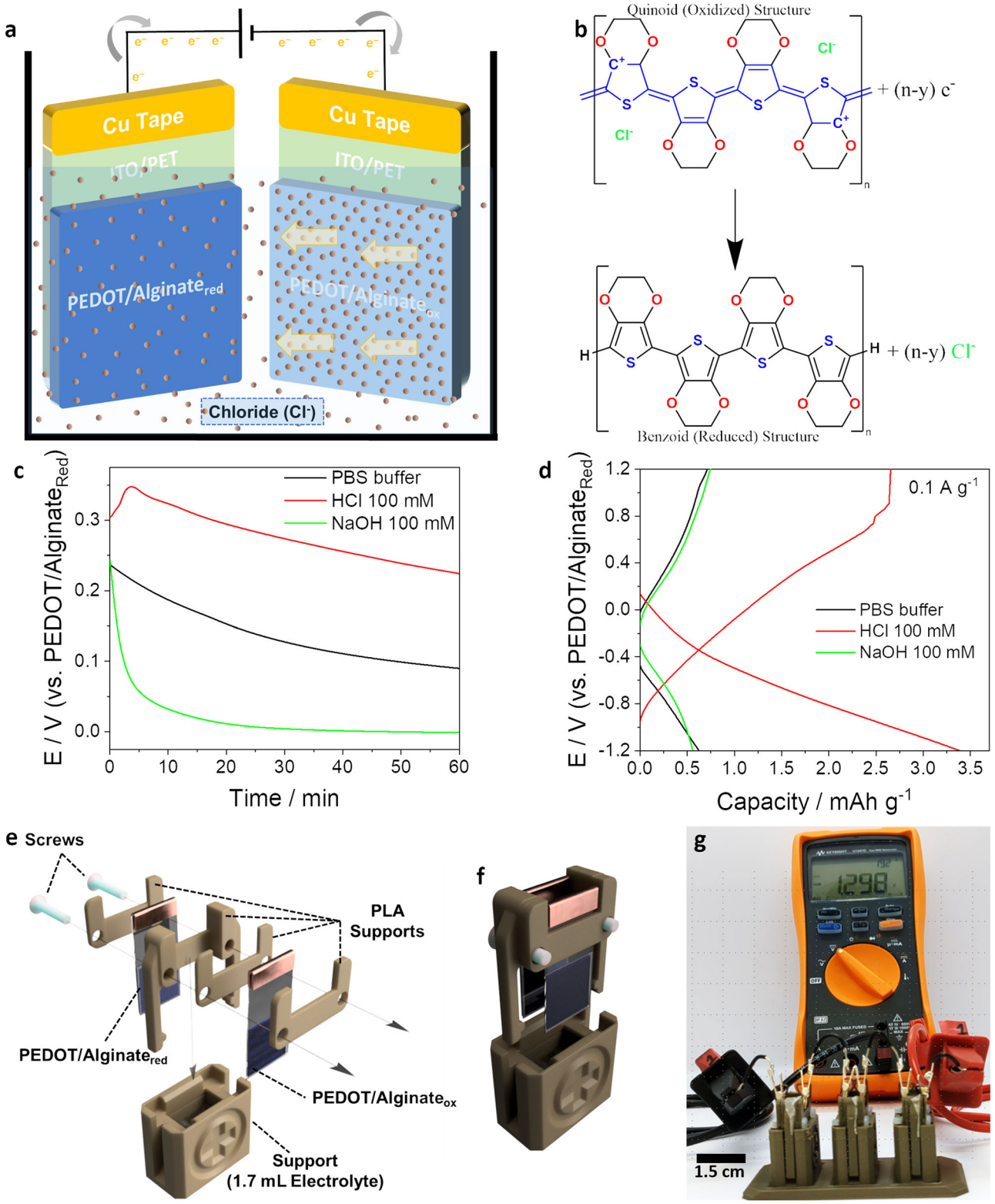

Fig. 6 | Wirelessly charged concentration cell battery. a Schematic representation of the single-cell battery design with chloride naturally diffusing from the wirelessly charged PEDOT/Alginate$_{ox}$. **b** Electrochemical half-cell cathodic reaction of PEDOT/Alginate$_{ox}$. **c** Electrical potential generated over time for different electrolyte solutions: PBS buffer (black), 100 mM hydrochloric acid (red), and 100 mM sodium hydroxide (green). **d** Galvanostatic charge-discharge curves for the different electrolytes at 0.1 A g^{-1}. **e** Schematic representation of the single-cell design using 3D-printed parts. **f** Schematic representation of an assembled single-cell. **g** Photograph of three single-cell batteries connected in series to a multimeter measuring the generated DC voltage.

BPE half compared to the ion concentration in the electrolyte creates a half-reaction resulting in a potential difference. Figure 6b illustrates the half-cell cathodic reaction for the oxidized half of the BPE. In this work, we focus solely on exploring the cathodic reaction since PEDOT is a p-type conducting polymer, and we use the reduced half (PEDOT/Alginate$_{red}$) solely to balance the charges. Figure 6c presents the evolution of the electric potential between the two halves of the BPE when immersed in common electrolytes. The best performance was observed with 100 mM hydrochloric acid (pH = 1.2), where a potential of nearly 350 mV was generated after 4 min. The potential then gradually decreases as the ionic concentration equilibrium is re-established. Immersed in PBS (pH = 7.4), the cell initially generated ~250 mV. In 100 mM sodium hydroxide (pH = 13.0) the cell initially generated ~250 mV but the potential here decayed faster than for all other electrolytes. The faradaic reaction involving PEDOT does not exhibit any pH dependence. However, the stability of the alginate hydrogel is strongly affected by pH[41–43]. Indeed, our results suggest that the stability of the alginate hydrogel plays a role in the evolution of the cell's potential, likely by impeding diffusion of Cl^- away from the PEDOT layer. The alginate hydrogel remains structurally intact in acidic environment (HCl, pH = 1.2, similar to gastric fluid) which results in slower cell discharge. At neutral pH (PBS, pH = 7.4, similar to intestinal fluid) Alginate begins to disassemble leading to faster cell discharge. Alginate exhibits an even higher degradation rate in basic environments (NaOH, pH = 13.0) leading to the fastest decay of the cell potential. The dependence of cell discharge rates on ambient pH can be further explored in applications where the gastrointestinal tract is investigated, for example using ingestible diagnostic devices[44].

Figure 6d depicts the galvanostatic charging–discharging curves for PEDOT/Alginate$_{ox}$ in various electrolytes at 0.1 A g^{-1}. Among them, 100 mM hydrochloric acid exhibited superior performance, achieving capacities of 2.7 mAh g^{-1} during charging and 3.3 mAh g^{-1} during discharging within the electrochemical window of 1.2 to −1.2 V. Figure 6e, f shows a schematic representation of a single-cell device, where we used 3D printed parts to hold the BPE halves in the electrolyte. Figure 6g shows a battery of three single-cells connected in series (Supplementary Movie 3). With three cells connected in series, we reached potentials of ~1.3 V. Currently, our concentration cell battery works with a half-cell reaction. Energy storage can be improved by adding an anodic half-cell reaction for example by using an n-type conducting polymer. Although direct comparisons are challenging, a recently reported edible battery cell utilizing ingredients like riboflavin and quercetin, demonstrated comparable potential (0.65 V) by employing both anodic and cathodic reactions in a single cell[45].

Our concentration cell utilizes the asymmetric distribution of small dopant ions encoded on PEDOT/Alginate coatings, by a wireless BE process. The wireless nature of BE could allow for multiple BPEs to be charged in parallel without complex wiring, potentially improving scalability and throughput in large-scale applications. The BE cells used here are similar to those used for water hydrolysis. This warrants further exploration of the feasibility of a hybrid process where green hydrogen/oxygen production is accompanied by wirelessly charging concentration cells.

Conclusions

In this study, we leveraged BE to wirelessly create reversible redox and chemical gradients in hybrid PEDOT/alginate hydrogel coatings. We explored application scenarios in controlled drug delivery and energy harvesting. We demonstrated wireless loading of concentration gradients of a model therapeutic molecule in both the PEDOT and hydrogel compartments of the BPE. Additionally, cutting and studying sections of the BPEs revealed distinct electroactive regions, which could serve as components of energy storage devices. These findings highlight the potential of BE for precise chemical modifications and wireless activation, paving the way for innovative applications in bioelectronics and energy.

Methods

Materials

The chemical reagents 3,4-ethylenedioxythiophene (EDOT), sodium alginate, calcium carbonate, SDS, TPP, fluorescein sodium salt were purchased from Sigma-Aldrich. All solutions were prepared with deionized Milli-Q water (18.2 MΩ cm) or with phosphate-buffered saline (PBS) pH 7.4 (Gibco™, Thermo Fisher Scientific, dilution 1×, osmolality 280–315 mOsm/kg).

Electrodeposition of BPEs

Flexible and conductive indium–tin oxide coated polyethylene terephthalate (ITO/PET, resistivity 60 Ω/sq, Sigma-Aldrich) were used as BPE base. For the PET/ITO/PEDOT/Alginate BPE the electrolyte composition was adapted from a previous work[37,46,47]. Firstly, 1.5% (w/w) of calcium carbonate (0.365 g) was dispersed in 24.3 mL of deionized water, followed by dissolution of 1% (w/w) sodium alginate kept under vigorous stirring for 30 min under room temperature. Later, 70 mM of SDS and 50 mM of EDOT was added. As soon as the EDOT was added, the solution was placed in an electrochemical cell for further electrodeposition. Key to obtaining homogeneous hydrogels was the maintenance of a uniform suspension of calcium carbonate microparticles in the electrolyte, which we ensured by constantly stirring the reaction solution (300 rpm in all experiments). For electropolymerization of PEDOT:SDS, the same procedure was executed without adding alginate and calcium carbonate. For PEDOT:TPP, 150 mM of TPP was added to the PEDOT:SDS solution. Further details can be found in Supplementary Movie 2. The BPEs (PEDOT:SDS, PEDOT:TPP and PEDOT/Alginate), all on PET/ITO substrates were prepared by applying +2.0 V (vs Ag/AgCl/KCl 3 M) for 120 s using CA method. The electrodeposition time was changed for obtaining different thickness.

Bipolar electrochemistry

The bipolar electrochemical cell was produced using a FDM 3D printer. The 'U' shape of the cell was adapted from previous work[6,7]. Two platinum plates of 10 mm × 12 mm were used as driving electrodes. The electrolyte solutions for BE activations were either 1 mM of NaCl or 1 mg mL^{-1} of fluorescein sodium salt. The BPE electrodes were 25 mm × 25 mm squares. Copper tape was used to improve electrical connection and avoid contact resistance to the ITO/PET substrate. The electrolyte immersed portion of the BPE had dimensions of 25 mm × 10 mm. BPEs were cut in a half resulting in two (12.5 mm × 25 mm) pieces where the reduced and oxidized BPE areas had dimensions of 12.5 mm × 10 mm. Further details can be found in Supplementary Movie 2. For BE activation, we used the chronopotentiometry method applying 2 mA constant current for 300 s (0.6 C) via the driving electrodes (Supplementary Fig. 7).

Electrochemical measurements

CV and EIS were performed using a potentiostat/galvanostat (PARSTAT3000, AMETEK) controlled using VersaStudio 2.60.2 software. CV traces were recorded in PBS as supporting electrolyte, from −1.2 V to +0.8 V (*vs* Ag/AgCl/KCl 3 M) using scan rate of 50 mV s^{-1}. EIS data were recorded from 1 MHz to 0.1 Hz, with excitation amplitude of 10 mV (RMS) at 10 points per decade. The BPE electrodes (halves) were the working electrode. A commercially available Ag/AgCl/KCl 3 M (BASi) electrode and a platinum coil were used as reference and counter electrodes, respectively.

Spectroscopic measurements

Raman spectra of the PEDOT:SDS$_{ox}$, PEDOT:SDS$_{red}$, PEDOT/Alginate$_{ox}$ and PEDOT/Alginate$_{red}$ were obtained using a WiTeC Alpha-R300 microscope equipped with a 633 nm laser with maximum power of 50 mW at the output. All the spectra were acquired with a 10×, long-distance objective in triplicate, sampling different parts of BPEs, with their normalized spectra shown as averages. The XPS analyses were carried out using a Kratos Supra instrument with a monochromatic aluminum source, and three analysis points per sample of (area 700 × 300 μm^2). Survey scans were collected between 1200 and 0 eV binding energy, at 160 eV pass

energy, 1 eV intervals, and 300 s/sweep with one sweep being collected. High-resolution O 1s, C 1s, Cl 2p, S 2p, and Ca 2p sweeps (for hydrogel BPEs only) were also collected at 40 eV pass energy and 0.1 eV intervals for each analysis point (one 300 s sweep for all except sulfur for which two 300 s sweeps for the S 2p transition were obtained).

Hydrogel characterization

For the wireless charge stored during the bipolar activation (Fig. 4f), the PEDOT/Alginate$_{ox}$ was charged by applying −0.8 V (vs Ag/AgCl/KCl 3 M) for 30 min, while the PEDOT/Alginate$_{red}$ was discharged by using +1.2 V (vs Ag/AgCl/KCl 3 M) for 30 min. Later, the BPEs were electronically reconnected using a new copper tape and placed back in the bipolar electrochemical cell as BPE electrode for a new cycle. The weight of the wet and dried PEDOT/Alginate layers were measured using a SM 625i-ION Semi-micro balance. The hydrogels were dried under room temperature overnight. The mass wet was obtained by: $m_{wet} = m_{hydrogel} - m_{ITO/PET}$. The mass dry was obtained by: $m_{wet} = m_{dried\ hydrogel} - m_{ITO/PET}$.

Controlled drug delivery

To quantify the concentration of the fluorescein molecule, a fluorescence spectrometer was used to measure light intensity. A reference curve was prepared using serial dilutions from 1 mg mL^{-1} to 1.5 10^{-5} mg mL^{-1}. Molecule excitation was at 485 nm and emission was measured at 528 nm. The concentration of fluorescein was calculated using the reference curve using GraphPad.

Wirelessly charged concentration cell

A BPE (PET/ITO/PEDOT/Alginate) was activated in the BE cell using sodium chloride 1 mg mL^{-1} as electrolyte. As described before the charge applied at the driving electrodes was 0.6 C. The BPE was cut in two halves. The halves were placed in a beaker containing electrolyte (HCl 100 mM, PBS or NaOH 100 mM) with the Alginate hydrogel layers facing each other. For the battery experiment, 3 cells were connected in series. Each cell was filled with 1.7 mL of HCl 100 mM (enough to cover the electrodes).

Statistical analysis

In bar graphs, bar heights indicate mean values, with error bars representing one standard deviation (S.D.), and horizontal lines indicating the median. Individual data points are shown for sample sizes $n < 10$. All graphs depict representative samples, each prepared in triplicate.

Data availability

The data that support the findings of this study are available from the corresponding author upon reasonable request.

Code availability

The G-code for the 3D-printing patterns are available from the corresponding authors upon request.

Received: 14 August 2024; Accepted: 30 January 2025;
Published online: 11 February 2025

References

1. Fosdick, S. E., Knust, K. N., Scida, K. & Crooks, R. M. Bipolar electrochemistry. *Angew. Chem. Int. Ed.* **52**, 10438–10456 (2013).
2. Ohira, M., Koizumi, Y., Nishiyama, H., Tomita, I. & Inagi, S. Synthesis of linear PEDOT fibers by AC-bipolar electropolymerization in a microspace. *Polym. J.* **49**, 163–167 (2017).
3. Watanabe, T. et al. In-plane growth of poly(3,4-ethylenedioxythiophene) films on a substrate surface by bipolar electropolymerization. *ACS Macro Lett.* **7**, 551–555 (2018).
4. Zhou, Y. et al. Template-free perpendicular growth of a poly(3,4-ethylenedioxythiophene) fiber array by bipolar electrolysis under an iterative potential application. *J. Mater. Chem. C* **7**, 14745–14751 (2019).
5. Koizumi, Y. et al. Electropolymerization on wireless electrodes towards conducting polymer microfibre networks. *Nat. Commun.* **7**, 10404 (2016).
6. Inagi, S., Ishiguro, Y., Atobe, M. & Fuchigami, T. Bipolar patterning of conducting polymers by electrochemical doping and reaction. *Angew. Chem. Int. Ed.* **49**, 10136–10139 (2010).
7. Ishiguro, Y., Inagi, S. & Fuchigami, T. Gradient doping of conducting polymer films by means of bipolar electrochemistry. *Langmuir* **27**, 7158–7162 (2011).
8. Carayon, I., Gaubert, A., Mousli, Y. & Philippe, B. Electro-responsive hydrogels: macromolecular and supramolecular approaches in the biomedical field. *Biomater. Sci.* **8**, 5589–5600 (2020).
9. Deng, Z., Yu, R. & Guo, B. Stimuli-responsive conductive hydrogels: design, properties, and applications. *Mater. Chem. Front.* **5**, 2092–2123 (2021).
10. Salinas, G., Arnaboldi, S., Garrigue, P. & Kuhn, A. Controlled patterning of complex resistance gradients in conducting polymers with bipolar electrochemistry. *Adv. Mater. Interfaces* **10**, 2202367 (2023).
11. Shi, Y. et al. High-throughput electrosynthesis of gradient polypyrrole film using a single-electrode electrochemical system. *Anal. Chem*. https://doi.org/10.1021/acs.analchem.2c04570 (2022).
12. Yan, Z.-B. et al. Bipolar electrodeposition of gradient polypyrrole films as a catalyst matrix for anodic ethanol oxidation. *Mater. Chem. Phys.* **277**, 125527 (2022).
13. Villani, E. & Inagi, S. Mapping the distribution of potential gradient in bipolar electrochemical systems through luminol electrochemiluminescence imaging. *Anal. Chem.* **93**, 8152–8160 (2021).
14. Zhou, Y., Shida, N., Tomita, I. & Inagi, S. Fabrication of gradient and patterned organic thin films by bipolar electrolytic micelle disruption using redox-active surfactants. *Angew. Chem. Int. Ed.* **60**, 14620–14629 (2021).
15. Ulrich, C., Andersson, O., Nyholm, L. & Björefors, F. Formation of molecular gradients on bipolar electrodes. *Angew. Chem. Int. Ed.* **47**, 3034–3036 (2008).
16. Bouffier, L., Zigah, D., Sojic, N. & Kuhn, A. Bipolar (Bio)electroanalysis. *Annu. Rev. Anal. Chem.* **14**, 65–86 (2021).
17. Karimian, N., Hashemi, P., Afkhami, A. & Bagheri, H. The principles of bipolar electrochemistry and its electroanalysis applications. *Curr. Opin. Electrochem.* **17**, 30–37 (2019).
18. Ma, Z. et al. Wireless magneto-ionics: voltage control of magnetism by bipolar electrochemistry. *Nat. Commun.* **14**, 6486 (2023).
19. Wang, H. et al. Bioelectrochemical remediation of Cr(VI)/Cd(II)-contaminated soil in bipolar membrane microbial fuel cells. *Environ. Res.* **186**, 109582 (2020).
20. Jain, A. et al. Wireless electrical–molecular quantum signalling for cancer cell apoptosis. *Nat. Nanotechnol.* **19**, 106–114 (2024).
21. Qin, C. et al. Data on enhanced wireless cell stimulation using soft and improved bipolar electroactive conducting polymer templates. *Data Brief* **43**, 108393 (2022).
22. Qin, C. et al. Enhanced wireless cell stimulation using soft and improved bipolar electroactive conducting polymer templates. *Appl. Mater. Today* **27**, 101481 (2022).
23. Qin, C., Yue, Z., Wallace, G. G. & Chen, J. Bipolar electrochemical stimulation using conducting polymers for wireless electroceuticals and future directions. *ACS Appl. Bio Mater.* **5**, 5041–5056 (2022).
24. Qin, C. et al. Bipolar electroactive conducting polymers for wireless cell stimulation. *Appl. Mater. Today* **21**, 100804 (2020).
25. Srinivasan, A., Roche, J., Ravaine, V. & Kuhn, A. Synthesis of conducting asymmetric hydrogel particles showing autonomous motion. *Soft Matter* **11**, 3958–3962 (2015).
26. Phuakkong, O. et al. Wireless synthesis and activation of electrochemiluminescent thermoresponsive janus objects using bipolar electrochemistry. *Langmuir* **32**, 12995–13002 (2016).

27. Ino, K. et al. Hydrogel electrodeposition based on bipolar electrochemistry. *Lab Chip* **18**, 2425–2432 (2018).
28. Xie, F., Li, C., Hua, X. & Ma, L. Biofabrication of controllable alginate hydrogel cell scaffolds based on bipolar electrochemistry. *J. Bioact. Compat. Polym.* **36**, 497–509 (2021).
29. Liu, L., Yellinek, S., Valdinger, I., Donval, A. & Mandler, D. Important implications of the electrochemical reduction of ITO. *Electrochim. Acta* **176**, 1374–1381 (2015).
30. Shi, H., Liu, C., Jiang, Q. & Xu, J. Effective approaches to improve the electrical conductivity of PEDOT:PSS: a review. *Adv. Electron. Mater.* **1**, 1500017 (2015).
31. Da Silva, A. C., Paschoal, V. H., Ribeiro, M. C. C. & de Torresi, S. I. C. Electrical/spectroscopic stability of conducting and biodegradable graft-copolymer. *Macromol. Chem. Phys.* **223**, 2200275 (2022).
32. Chiu, W. W., Travaš-Sejdić, J., Cooney, R. P. & Bowmaker, G. A. Studies of dopant effects in poly(3,4-ethylenedi-oxythiophene) using Raman spectroscopy. *J. Raman Spectrosc.* **37**, 1354–1361 (2006).
33. Nešpůrek, S. et al. Raman spectroscopy and DFT calculations of PEDOT:PSS in a dipolar field. *Phys. Chem. Chem. Phys.* **24**, 541–550 (2022).
34. Thomas, J. P. et al. Reversible structural transformation and enhanced performance of PEDOT:PSS-based hybrid solar cells driven by light intensity. *ACS Appl. Mater. Interfaces* **7**, 7466–7470 (2015).
35. Alhummiany, H., Rafique, S. & Sulaiman, K. XPS analysis of the improved operational stability of organic solar cells using a V 2 O 5 and PEDOT:PSS composite layer: effect of varied atmospheric conditions. *J. Phys. Chem. C* **121**, 7649–7658 (2017).
36. Cassinelli, M. et al. Rationalizing the enhancement of the thermoelectric properties of PEDOT:PSS by secondary doping. *Appl. Phys. Lett*. **119**, 033301 (2021).
37. Da Silva, A. C., Paterson, T. E. & Minev, I. R. Electro-assisted assembly of conductive polymer and soft hydrogel into core-shell hybrids. *Soft Sci.* **3**, 3 (2023).
38. Kingsbury, R. S., Chu, K. & Coronell, O. Energy storage by reversible electrodialysis: the concentration battery. *J. Memb. Sci.* **495**, 502–516 (2015).
39. van Egmond, W. J., Starke, U. K., Saakes, M., Buisman, C. J. N. & Hamelers, H. V. M. Energy efficiency of a concentration gradient flow battery at elevated temperatures. *J. Power Sources* **340**, 71–79 (2017).
40. Luo, J. et al. Unraveling pH dependent cycling stability of ferricyanide/ferrocyanide in redox flow batteries. *Nano Energy* **42**, 215–221 (2017).
41. Lima, D. S. et al. pH-responsive alginate-based hydrogels for protein delivery. *J. Mol. Liq.* **262**, 29–36 (2018).
42. Lin, X. et al. Dual-responsive alginate hydrogels for controlled release of therapeutics. *Molecules* **24**, 2089 (2019).
43. Pawar, S. N. & Edgar, K. J. Alginate derivatization: a review of chemistry, properties and applications. *Biomaterials* **33**, 3279–3305 (2012).
44. Moglia, A., Menciassi, A., Dario, P. & Cuschieri, A. Capsule endoscopy: progress update and challenges ahead. *Nat. Rev. Gastroenterol. Hepatol.* **6**, 353–361 (2009).
45. Ilic, I. K. et al. An edible rechargeable battery. *Adv. Mater*. **35**, 2211400. (2023).
46. Da Silva, A. C., Wang, J. & Minev, I. R. Electro-assisted printing of soft hydrogels via controlled electrochemical reactions. *Nat. Commun.* **13**, 1353 (2022).
47. Da Silva, A. C. et al. Electrochemically driven assembly of chitosan hydrogels on PEDOT surfaces. *Macromol. Mater. Eng*. https://doi.org/10.1002/mame.202300263 (2023).

Acknowledgements

The authors acknowledge Dr. Deborah Hammond (University of Sheffield Surface Analysis Center) for assistance with XPS analysis. They thank FAPESP (grants 2019/00207-0 and 2022/11983-4), CNPq (grant 303045/2021-3), and the Insigneo Institute for in silico Medicine for student scholarships. This work was also supported by the ERC Starting Grant IntegraBrain (804005).

Author contributions

A.C.D.S. conceived the idea and analyzed the results. A.C.D.S. and X.H. planned and performed most of the experiments. V.H.P. and M.C.C.R. did the Raman analysis. A.J.Z. performed the fluorescein quantification analysis. A.C.D.S. and N.H. performed the battery experiments. A.C.D.S. and I.R.M. wrote the paper.

Funding

Open Access funding enabled and organized by Projekt DEAL.

Competing interests

The authors declare no competing interests.

Additional information

Supplementary information The online version contains supplementary material available at https://doi.org/10.1038/s43246-025-00750-1.

Correspondence and requests for materials should be addressed to Aruã Clayton Da Silva or Ivan Rusev Minev.

Peer review information *Communications Materials* thanks Serena Arnaboldi and the other, anonymous, reviewer(s) for their contribution to the peer review of this work. Primary Handling Editors: Ruben Rizo and Jet-Sin Lee. A peer review file is available.